Computers and Electronics in Agriculture 152 (2018) 74–81

Contents lists available at ScienceDirect

Computers and Electronics in Agriculture

journal homepage: www.elsevier.com/locate/compag

Unmanned aerial system assisted framework for the selection of high yielding cotton genotypes

Jinha Jung[a,*], Murilo Maeda[b], Anjin Chang[a], Juan Landivar[b], Junho Yeom[a], Joshua McGinty[c]

[a] Texas A&M University – Corpus Christi, 6300 Ocean Drive, Corpus Christi, TX 78412, United States
[b] Texas A&M AgriLife Research, 10345 State Hwy 44, Corpus Christi, TX 78406, United States
[c] Texas A&M AgriLife Extension, 10345 State Hwy 44, Corpus Christi, TX 78406, United States

ARTICLE INFO

Keywords:
Unmanned Aerial System
Precision agriculture
High throughput phenotyping
Breeding selection
Remote sensing

ABSTRACT

Recent advances in molecular breeding and bioinformatics have greatly accelerated the screening of large sets of genotypes. Development of field-level phenotyping, however, still lags behind and is considered by many as the main bottleneck to improved efficiency in breeding programs. Unmanned Aerial System (UAS) and sensor technology available today enables collection of data at high spatial and temporal scales, previously unobtainable using traditional airborne remote sensing technologies. Here, we propose an UAS-assisted high throughput phenotyping framework for cotton (*Gossypium hirsutum* L.) genotype selection. UAS data collected on July 24, 2015 were used to calculate canopy cover, and UAS data collected on August 5, 2015 were used to extract open boll related phenotypic features including number of open bolls, average area of open bolls, average diameter of open bolls, perimeter of open bolls, perimeter to area ratio. Using the extracted features, a sequential selection procedure was performed on a population of 144 entries. Entries selected from the proposed framework were compared to the highest yielding entries determined by mechanical harvest results. Experimental results indicated that the selection process increased minimum and average lint yield of the remaining population by 7.4 and 10%, respectively, and UAS-selected entries and genotypes matched 80 and 73%, respectively, the same lists ranked by actual field harvest measurements.

1. Introduction

Currently, cotton (*Gossypium* sp.) is the world's most important natural textile fiber crop, accounting for around 35 percent of total world fiber use. Also, it is one of the biggest crops in the food oil industry (USDA, http://www.ers.usda.gov/topics/crops/cotton-wool.aspx). Plant breeding is one of civilization's oldest activities and started with the need of improving plants for human benefit. Today, the world's food, feed, and fiber production relies on breeding programs to create genetic types that excel in productivity and meet population needs. To that end, molecular plant breeding techniques and bioinformatics have significantly evolved in the past few decades (Cabrera-Bosquet et al., 2012; Hulse-Kemp et al., 2014; Mayes et al., 2005; Yu et al., 2014) to develop cotton genotypes with higher potential yield. The advancement of high throughput genotyping platforms and the access to fast and relatively inexpensive genomic information revolutionized cotton breeding programs. The ability to work efficiently in a genomic level enabled fast advances in innumerous sectors of genetic research. In plant breeding, the use of genetic maps and molecular markers in marker assisted selection to meticulously target the gene/trait of interest greatly expedites the breeding process. Phenotyping, on the other hand, has not developed at the same pace, despite its important role in plant breeding research (Araus and Cairns, 2014). Lack of high-throughput phenotyping method is known to be the main bottleneck for increased breeding efficiency, and current phenotyping methods still remain relatively low throughput, laborious, and time-consuming. Efficient, rapid, and reliable high throughput phenotyping platforms are much needed to decrypt relationship between the full suite of genetic and environmental factors and phenotypic variations at plant- and population-levels (Cobb et al., 2013; Furbank and Tester, 2011).

Traditionally, a plant breeding program focuses on several major steps. First, breeders establish the goal(s) of his program with a defined objective to focus their attention in gathering and/or creating a breeding population (genetic variability). After a base population has been established, one needs to choose one, or a combination of several available breeding strategies to deal with the segregating populations (e.g. pedigree, modified bulk, backcross, etc). Finally, based on the goal

* Corresponding author.
E-mail address: jinha.jung@tamucc.edu (J. Jung).

https://doi.org/10.1016/j.compag.2018.06.051
Received 15 February 2018; Received in revised form 18 June 2018; Accepted 29 June 2018

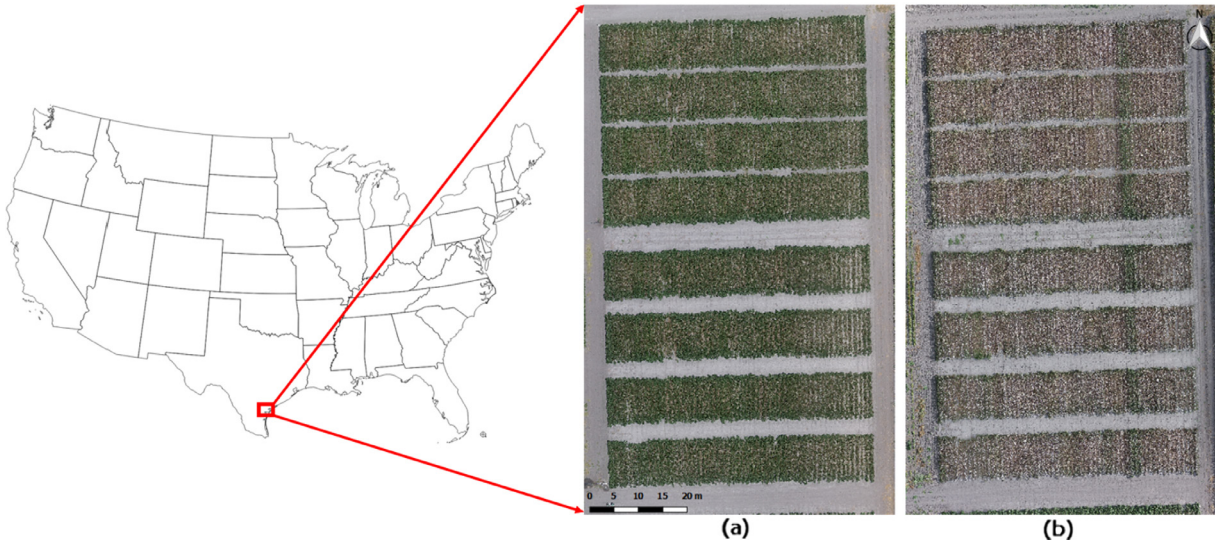

Fig. 1. Location of the study site and orthomosaic images of the field (1) on July 24, 2015 when canopy was fully developed and (b) on August 5, 2015 after defoliation.

(s) of the breeding program, stable non-segregating superior genotypes are identified to be commercially released to the public. Typically, multiple years of intense screening and selection are required to develop and bring new elite genetic types or "cultivars" to market. As a result of the expansion of breeding programs and an increase of demand by the world's population, breeders are always searching for new methods to increase efficiency, and convenient techniques to facilitate the breeding process.

Although traditional satellite remote sensing technologies have been utilized to address issues in effectively selecting high yield genotypes, the lack of spatial resolution and limited temporal resolution due to their orbital design were mentioned as key hurdles in enabling breeding selection framework using the remote sensing technologies (Berni et al., 2009). Recent advances in sensor technologies now made it possible to integrate small and lightweight sensors into Unmanned Aerial System (UAS). In the early stage of UAS technology for agriculture applications, most research focused on developing UAS data processing scheme and accessing data accuracy. Honkavaara et al. (2013) investigated the processing and uses of UAS image data in precision agriculture. They developed a processing scheme from raw images up to georeferenced reflectance image and digital surface models. The results confirmed that UAS technology has a great potential in precision agriculture and indicated many possible future researches. Gómez-Candón et al. (2014) studied geometric accuracy and crop line alignment while taking into account three different flight altitudes and a different number of GCPs. The results concluded that UAS data collection at a range between 30 and 100 m altitude and using a moderate number of GCPs can result in ultra-high resolution orthomosaic images. Rokhmana (2015) investigated the potential of UAS-based remote sensing for precision agriculture. The system used in the study has the ability to produce imagery with spatial resolution of < 10 cm and the average geometric accuracy can be obtained up to 3 pixels, while the production time can be reached more than 500 ha a day. Primicerio et al. (2012) tested autonomous UAS flight for multispectral UAS image acquisition and the acquired images showed good agreement with ground-based spectrometer data.

In addition to the previous literatures, more detailed precision agriculture studies using UASs have been conducted to extract phenotypic features from the UAS data. Gevaert et al. (2015) combined multispectral satellite imagery with hyperspectral UAS imagery for precision agriculture applications for the first time. They constructed spectral-temporal response surfaces for crop phenology monitoring. Gago et al. (2015) compared the performance of different types of UASs with ground-truth plant data in terms of crop water stress. The results showed that thermal indices have a great potential to determine water stress heterogeneity. López-Granados et al. (2016) generated georeferenced weed seedling infestation maps by analyzing of visible and near-infrared UAS images. Based on the classification map, they investigated variability of herbicide treatments against weed coverage ratio. Bendig et al. (2015) combined selected vegetation indices and plant height information to estimate crop biomass. The correlations between vegetation indices and dry biomass were analyzed and then multiple regression models using selected vegetation indices and plant height were developed.

UAS can perform aerial data acquisition missions without manual control. To address the limitations of traditional remote sensing technologies, we propose to utilize an Unmanned Aerial System (UAS) as a data acquisition platform and develop a framework to select high yield cotton genotypes based on measurements from the UAS data. The main objectives of this study is to develop a systematic framework to select high yield cultivars using data acquired from UAS so that the developed framework can be used to empower breeders to improve their cultivar selection process.

2. Methods

2.1. Study site

A dryland field trial was established at the Texas A&M AgriLife Research and Extension Center (27° 46.948′N, 97° 33.605′W, elevation 16 m above sea level) at Corpus Christi, TX during the summer of 2015 (Fig. 1). The dryland field trial was approximately 35 m in width and 110 m in height. Seeds of 48 different cotton genotypes were planted on March 27, 2015 at a rate of 13.3 *seeds/m* in north to south oriented rows. Crop emergence occurred six days later on April 2, 2015. Plots were arranged in a randomized complete block design and each genotype was replicated three times, for a total of 144 plots. Each plot consisted of two rows that were 10.7 m long spaced at 0.96 m. Management practices such as fertility, disease prevention, weed and insect control followed the guidelines recommended by local Texas A&M AgriLife Extension specialists. Harvest aids were applied when cotton plants exhibited approximately 60% open bolls, and consisted of a combination of thidiazuron (*N*-phenyl-*N*-1,2,3-thidiazol-5-ylurea; 0.025 kg a.i. ha^{-1}) and diuron (3-(3,4-dichlorophenyl)-1,1-dimethylurea; 0.013 kg a.i. ha^{-1}) for defoliation, and ethephon (2-chloroethyl phosphonic acid; 0.59 kg a.i. ha^{-1}) and cyclanilide (1-(2,4-

Table 1
Summary statistics of genotypes' lint yield.

Genotype	Replications	Mean Lint Yield[a]	Std. Dev	Std. Err. Mean	Lower 95%	Upper 95%
PHY312WRF	3	1608.0	285.5	164.8	898.8	2317.3
P11X3311	3	1595.1	136.8	79.0	1255.3	1934.8
P12X4841	3	1550.6	121.9	70.4	1247.9	1853.3
P11X3305	3	1545.2	201.8	116.5	1043.9	2046.5
ST4946GLB2	3	1541.5	237.6	137.2	951.2	2131.8
P12X4833	3	1535.6	103.8	59.9	1277.8	1793.5
P12X3419	3	1487.7	80.1	46.2	1288.8	1686.5
P10X4699	3	1485.7	357.9	206.6	596.7	2374.6
PHY333WRF	3	1470.7	129.3	74.7	1149.5	1792.0
P11X3289	3	1445.8	26.5	15.3	1379.9	1511.8
P12X3417	3	1427.7	177.1	102.3	987.7	1867.7
P11X4760	3	1409.4	116.0	67.0	1121.2	1697.5
P06X.3122	3	1406.0	90.9	52.5	1180.1	1631.8
P07X.5540	3	1405.4	265.2	153.1	746.7	2064.1
P12X51257	3	1395.3	281.6	162.6	695.8	2094.8
PHY339WRF	3	1390.5	70.6	40.8	1215.0	1565.9
P07X.4444	3	1387.7	132.0	76.2	1059.7	1715.7
P11X3308	3	1387.0	156.3	90.3	998.7	1775.4
P12X4840	3	1383.6	208.1	120.2	866.6	1900.7
PHY496W3F	3	1379.7	42.5	24.6	1274.0	1485.4
P12X3393	3	1375.5	334.1	192.9	545.5	2205.5
DP1321B2RF	3	1349.2	300.7	173.6	602.2	2096.2
P10X3249	3	1347.3	216.0	124.7	810.7	1883.9
PHY487WRF	3	1336.6	336.2	194.1	501.3	2171.9
P12X3394	3	1335.7	70.1	40.5	1161.4	1509.9
PX4533-18WRF	3	1327.7	86.5	50.0	1112.8	1542.6
PHY444WRF	3	1318.0	167.2	96.5	902.8	1733.3
ST4747GLB2	3	1302.8	132.3	76.4	974.1	1631.5
PHY495W3F	3	1300.5	271.2	156.6	627.0	1974.1
P11X51121	3	1300.5	234.2	135.2	718.7	1882.2
PHY552WRF	3	1283.1	89.7	51.8	1060.3	1505.9
P09X4569	3	1281.5	69.5	40.2	1108.7	1454.2
P04X.3074	3	1278.6	110.9	64.0	1003.1	1554.1
P11X51166	3	1271.9	193.2	111.5	792.0	1751.8
P12X51286	3	1263.3	91.2	52.7	1036.7	1489.9
P12X51332	3	1246.1	370.7	214.0	325.1	2167.0
P12X51240	3	1236.3	274.7	158.6	554.0	1918.6
PX5590-01WRF	3	1225.3	169.1	97.7	805.2	1645.4
P12X51287	3	1220.8	151.7	87.6	844.0	1597.5
P12X51322	3	1207.7	172.1	99.4	780.3	1635.2
DP1252B2RF	3	1189.6	312.4	180.4	413.5	1965.7
PHY427WRF	3	1189.3	82.2	47.5	985.1	1393.5
P11X51185	3	1171.0	14.6	8.5	1134.6	1207.3
NG1511B2RF	3	1164.6	141.1	81.5	814.1	1515.1
PHY499WRF	3	1113.1	93.3	53.9	881.4	1344.7
DP1454NRB2RF	3	1108.0	317.3	183.2	319.8	1896.3
ST6448GLB2	3	1076.9	118.9	68.7	781.6	1372.3
P10X4689	3	1076.3	72.5	41.8	896.3	1256.3

[a] Lint Yield (kg/ha).

dichlorophenylaminocarbonyl)-cyclopropane carboxylic acid); 0.037 kg a.i. ha^{-1}) for opening closed bolls. All plots were harvested using a custom 2-row cotton spindle picker model 9900 (Deere & Company, Moline, IL) on August 10, 2015. This equipment was modified for small-plot research and allowed yield to be established on a per plot basis. A sub-sample of approximately 400 g from each plot was collected and ginned to determine lint yield and gin turnout. Table 1 summarizes lint yields of genotypes tested in this study. Average lint yields ranged from 1076.3 kg/ha to 1608.0 kg/ha.

2.2. UAS data acquisition and pre-processing

Small Unmanned Aerial System (sUAS) - DJI Phantom 2 Vision Plus (DJI Technology, Shenzhen, China) - was utilized to acquire aerial images over the test field. The aerial platform is lightweight, approximately 1.2 kg with battery, propellers, and camera onboard. The UAS platform has a flight endurance of up to 25 min with a single battery and can cover approximately 6 ha in a single flight. It is equipped with a 1/2.3″ sensor and its resolution is 14 Mega pixels (4383 × 3288 pixels) with 110° horizontal and 85° vertical field of view. It is capable of performing autonomous flights with the guidance of a GPS sensor onboard, given pre-programmed flight paths are provided in advance.

Aerial data acquisition was conducted on July 24, 2015 when cotton canopy was almost fully developed and on August 5, 2015 after the crop had been defoliated and open bolls were more visible. The earlier flight data was used to estimate canopy cover of individual genotype and the later flight data were used to perform open cotton boll count analysis. The UAS was programmed to perform data collection at 30 m altitude above ground with 85% image overlap, and total flight time of the data acquisition was 11 min and 14 s. A total of 4 ground control points (GCPs) were installed around the edge of the study field and their precise locations were surveyed using an APS-3 RTK (Real Time Kinematic) GPS device, manufacture by Altus Positioning Systems Inc. (California, USA), for accurate georeferencing of orthomosaic images. The aerial data acquisition mission was designed using Pix4D capture application (see https://pix4d.com/product /pix4dcapture-app/), and it resulted in 142 raw images. Although geographical locations (longitude, latitude, and altitude) of the raw images were also recorded for

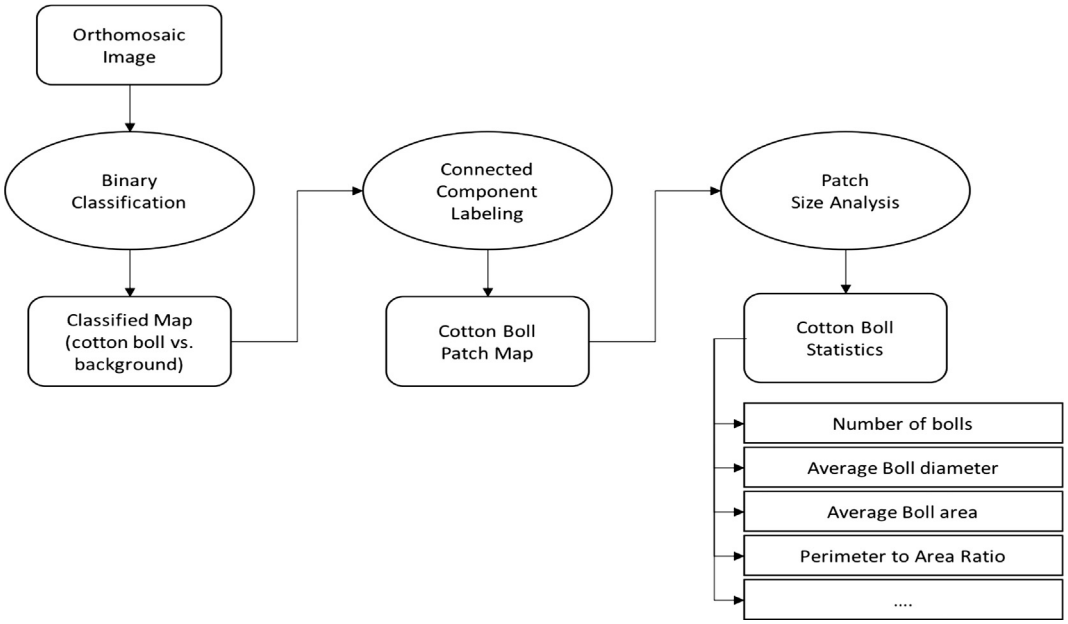

Fig. 2. Open cotton boll analysis workflow.

initial processing, onboard GPS sensor in the UAS did not provide high enough accuracy for direct georeferencing. The surveyed GCPs were utilized to improve georeferencing accuracy of the final geospatial products. The raw images were processed using Agisoft Photoscan Pro (see http://www.agisoft.com) Structure from Motion (SfM) software to generate geospatial data products such as an orthomosaic image, 3D point cloud data, and Digital Elevation Model (DEM). The spatial resolution of the resulting orthomosaic image and the DEM was 0.87 cm and 1.74 cm, respectively.

2.3. Open cotton boll count analysis

A new algorithm to count open cotton boll from an orthomosaic image was developed. Thanks to low flying altitude of UAS platforms, very high resolution (sub centimeter resolution) orthomosaic images can be generated make it possible to delineate individual cotton boll from background. The developed open boll count algorithm consists of three major steps (Fig. 2).

During the first step of the process, a binary classification of the orthomosaic image was performed to differentiate open cotton bolls from background objects. Visual inspection of each band showed that the red band presented the greatest separation between open cotton bolls and background objects. A single band (Red) of the orthomosaic image was used for the classification. The orthomosaic image was generated with 8-bit precision and their digital value ranges from 0 to 255. The threshold value of 190 was chosen to perform the binary image classification after visual inspection of the boundaries between cotton bolls and background objects. The classified image was then fed into a connected component labeling algorithm. The second step of the analysis is to identify the cluster from individual cotton bolls from the classification results. A connected component labeling (Rosenfeld and Pfaltz, 1966) algorithm with 4 connectivity rule was used to identify connected patches. A unique ID number was assigned to individual patches for later analysis. The third step of the analysis workflow is to perform patch size analysis to calculate spatial characteristics of open cotton bolls including centroid, area, eccentricity, equivalent diameter, perimeter, and perimeter to area ratio. Fig. 3 illustrates example results of the open cotton boll analysis. The spatial characteristics of individual cotton bolls were then summarized for each plot for later analysis.

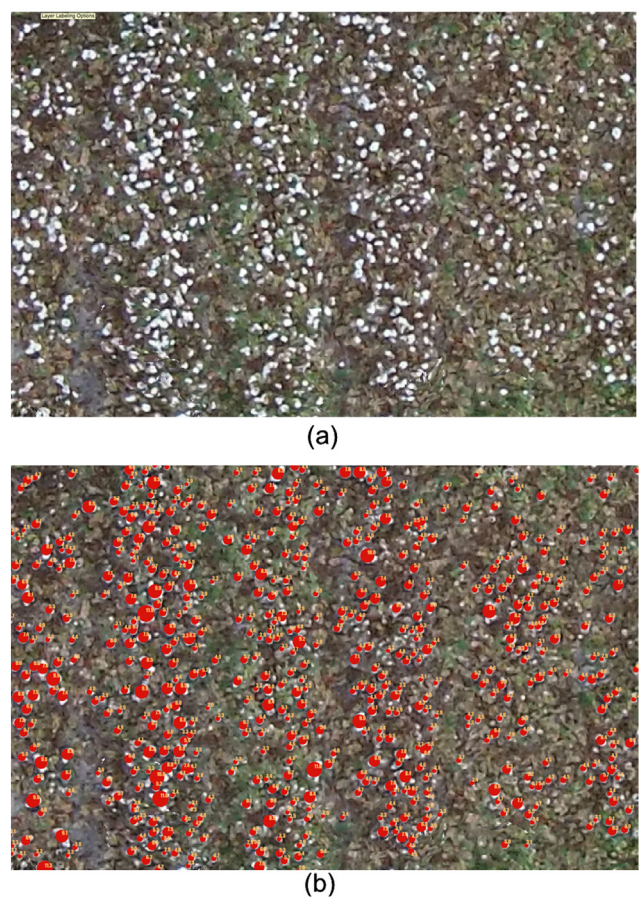

Fig. 3. Example results of open cotton boll analysis: (a) orthomosaic image, (b) open cotton boll analysis results (red circle is placed at the centroid of each boll and radius of the circle is proportional to equivalent diameter).

2.4. Canopy cover estimation

Canopy cover is a critical phenotype for cotton since it represents leaf surface area to capture sun light for photosynthesis. The

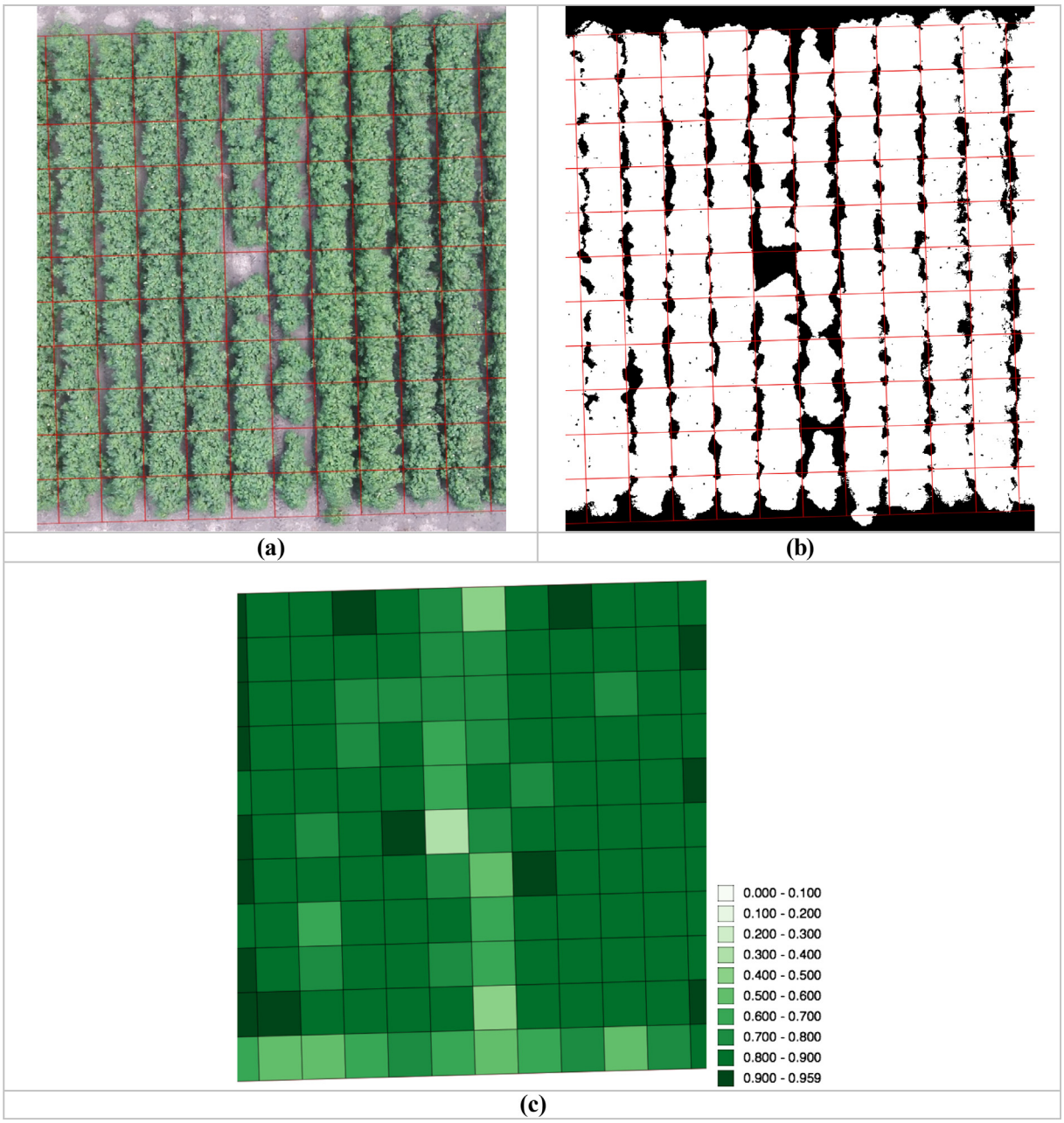

Fig. 4. Canopy cover estimation from the orthomosaic images (Red square: individual crop grid, and each grid is 0.97 m in square): (a) a natural color orthomosaic image acquired from UAS platform, (b) binary classification results of the orthomosaic image (white: canopy class, black: non-canopy class), (c) estimated canopy cover.

Table 2
UAS variables used in the genotype selections. Variables were chosen according to their potential contribution to cotton yield.

Linear Fit	R^2	RMSE[a]
lint (kg/ha) = −1758.406 + 2005.2014 * log(***MEBD***)	0.31	173.4
lint (kg/ha) = −1835.9 + 1160.6 * log(***MBP***)	0.30	175.5
lint (kg/ha) = −1233.3 + 873.3 * log(***MBA***)	0.31	173.8
lint (kg/ha) = −1296.1 + 75.1 * ***MCC***	0.0021	209.01

[a] RMSE: Root mean square error.

Table 3
Description of the selection procedure.

Sel. Cycle	Variable Used	Selection Description	Number of Entries
Original	N/A	Original population	144
1	MEBD	Removed lower 28 entries from the list	116
2	MBP	Removed lower 28 entries from the list	88
3	MBA	Removed lower 28 entries from the list	60
4	MCC	Removed lower 28 entries from the list	32

Table 4
Changes in lint yield of the population based on selections using UAS variables.

Sel. cycle	Variable used	Number of Entries	Lint yield			Change from original population		
			Min. kg ha^{-1}	Avg. kg ha^{-1}	Max. kg ha^{-1}	Min. %	Avg %.	Max. %
Original	N/A	144	923	1336	1884	0	0	0
1	MEBD	116	927	1379	1884	0.4	3.2	0
2	MBP	88	991	1411	1884	7.4	5.6	0
3	MBA	60	991	1451	1884	7.4	8.6	0
4	MCC	32	991	1470	1884	7.4	10.0	0

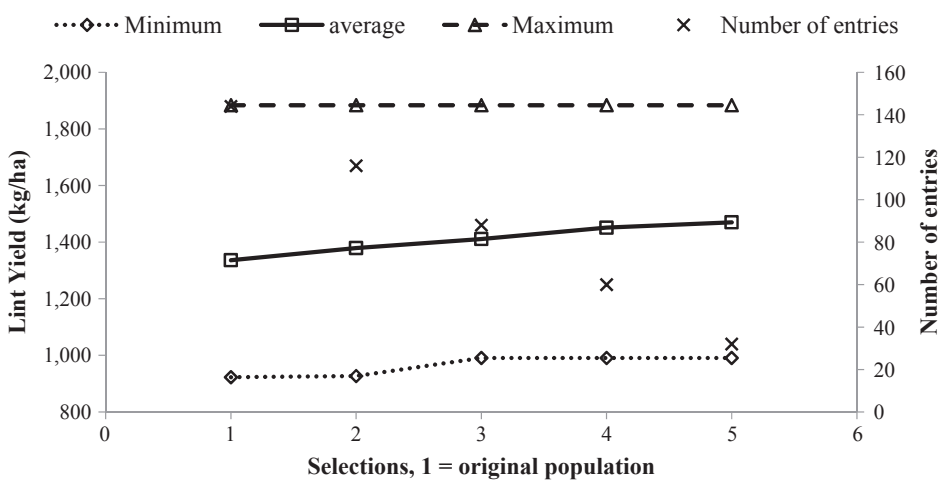

Fig. 5. Genotype selection based on UAS-derived variables. In each selection round 28 entries were removed. Selections 2, 3, 4, and 5 were based on mean equivalent boll diameter, mean boll perimeter, mean boll area, and mean canopy cover, respectively. Dashed, solid, and dotted lines represent maximum, average, and minimum lint yield of the population, respectively.

Table 5
Summary of final selected entries based on field harvest measurements (a.) and UAS open cotton boll analysis measurements (b.). Table shows the top 5 high-yielding entries on a plot by plot basis.

(a.) Harvest					(b.) UAS				
Rank	Genotype	Plot	Rep.[b]	Lint Yield[a]	Rank	Genotype	Plot	Rep.[b]	Lint Yield[a]
1	P10X4699	114	1	1884	1	P10X4699	114	1	1884
2	ST4946GLB2	107	1	1788	2	PHY312WRF	215	2	1777
3	PHY312WRF	215	2	1777	3	PHY312WRF	132	1	1768
4	PHY312WRF	132	1	1768	4	P11X3305	137	1	1758
5	P11X3305	137	1	1758	5	P12X51257	124	1	1693

[a] Lint yield shown in kg ha^{-1}.
[b] Indicates which replication the entry came from.

orthomosaic image was used to estimate canopy cover for each genotype. First, the orthomosaic image was classified into canopy and non-canopy classes by applying the Canopeo algorithm (Patrignani and Ochsner, 2015). Individual crop grid whose dimension is 0.96 m by 0.96 m was defined along planting direction, and each plot consisted of two rows that were 10.7 m long. This resulted in 22 individual crop grids within each plot. Canopy cover within the individual crop grid was calculated by dividing canopy pixel by the total number of pixel in each crop grid (Fig. 4), and average of 22 canopy cover value (*Mean Canopy Cover*) was assigned as canopy cover estimates for each genotypes.

3. Results and discussion

3.1. Genotype/Entry selection process

The field trial included breeding lines (32) and commercially available varieties (16), for a total of 48 genotypes. Phenotypic features extracted from the UAS data were summarized by each genotype. Among the summarized features, four variables - mean equivalent boll diameter (MEBD), mean boll perimeter (MBP), mean boll area (MBA), and mean canopy cover (MCC) - were chosen based on preliminary regression analysis for their correlation with final harvested lint yield (Table 2) so that these features can be used to select high yielding varieties in the next step. All variables were log-transformed (natural logarithm) prior to the selection process, with the exception of the mean canopy cover variable. We adopted a sequential selection approach to select high yielding varieties. A sequential selection process with 4 stages were made based solely on the open cotton boll analysis results, which did not include yield data per se other than for the preliminary analysis of variables. For each round of selection, the sequential selection approach ranks genotypes using the models developed in Table 2, and the lowest 28 entries (approximately 19% of the original population) were removed (Table 3). For the purpose of the UAS-based selection procedure each plot was considered as an individual entry (i.e. total of 144).

Selection stages increased the minimum and average lint yield among the remaining population (Table 4). After the final selection, minimum lint yield of the population increased by 7.4% and average lint yield increased by 10% compared to the original population, prior to the selection process (Fig. 5).

As a result of the sequential selection, 32 entries remained in the

Table 6
Summary of final selected genotypes based on field harvest measurements (a.) and UAS open cotton boll analysis measurements (b.). Table shows top 15 high-yielding genotypes. Field measurements table show the mean lint yield of each genotypes for 3 replications (a.). UAS open cotton boll analysis measurements show lint yield or mean lint yield depending how many replications were selected (b.).

(a.) Harvest				(b.) UAS			
Rank	Genotype	Reps.	Mean Lint Yield[a]	Rank	Genotype	Reps.	Lint Yield[b]
1	PHY312WRF	3	1608	1	PHY312WRF	2	1773
2	P11X3311	3	1595	2	P11X3305	1	1758
3	P12X4841	3	1551	3	P12X4833	1	1633
4	P11X3305	3	1545	4	P10X4699	2	1633
5	ST4946GLB2	3	1541	5	P12X3417	1	1626
6	P12X4833	3	1536	6	P10X3249	1	1571
7	P12X3419	3	1488	7	P11X4760	1	1542
8	P10X4699	3	1486	8	P12X51240	1	1538
9	PHY333WRF	3	1471	9	P12X51257	2	1526
10	P11X3289	3	1446	10	P11X3311	1	1488
11	P12X3417	3	1428	11	DP1454NRB2RF	1	1474
12	P11X4760	3	1409	12	P11X3289	1	1458
13	P06X.3122	3	1406	13	P12X4841	1	1443
14	P07X.5540	3	1405	14	P07X.5540	1	1431
15	P12X51257	3	1395	15	P11X51121	2	1425

[a] Mean lint yield of 3 replications shown in kg ha^{-1}.
[b] Lint yield or mean lint yield if replications is greater than 1, shown in kg ha^{-1}.

final population. These entries were selected solely based on phenotypic features extracted from the open cotton boll analysis and canopy cover estimations, as described earlier. When plots were ranked by actual harvested lint yield, only PHY312WRF appeared more than once in the top 5 list (Table 5.a.). The top 5 UAS-selected plots ranked by lint yield also contained PHY312WRF twice (Table 5.b.). Overall, by reducing the original population from 144 plots to the top 5, 4 out of 5 plots were present in both UAS and field harvest lists, which represent an accuracy of 80% for the UAS-based selection procedure (Table 5).

On a slightly different scenario, the top 15 genotypes (not plots) were ranked by lint yield and compared to an UAS-selected genotype list (Table 6). Table 6.a. shows the mean lint yield of 3 replications for the top 15 ranked genotypes, from highest to lowest yielding. On the UAS side, the mean lint yield of the final 32 plots from the step-wise selection procedure previously described (Tables 3 and 4) were calculated, which resulted in a list of 24 individual genotypes. From those, 15 genotypes were selected for comparison with the harvested lint yield list (Table 6.b.). For this scenario 11 out of 15 genotypes were present in both lists, which represent 73% accuracy. Genotypes PHY312WRF, P10X4699, P12X51257, and P11X51121 were selected twice through the UAS-selection procedure and therefore mean lint yield of two replications is shown for those (Table 6.b.). Remaining genotypes were only selected once, thus lint yield is shown for the particular replication chosen.

4. Conclusion

In conclusion, here we briefly demonstrate the potential of UAS technology and advanced image analysis techniques to facilitate cotton breeding efforts. By utilizing UAS-derived information regarding open cotton bolls and canopy cover, a four-step selection process for high yielding entries was performed. Ultimately, the selection process increased minimum and average lint yield of the remaining population by 7.4 and 10%, respectively. UAS-selected entries and genotypes matched 80 and 73%, respectively, the same lists ranked by actual field harvest measurements. It is important to notice, however, that this technology and associated methodologies are not intended, by any means, to replace the plant breeder. Rather, breeders should consider this emerging technology as a powerful tool to help accelerate the screening of a large number of genotypes, bridging the gap between genomics and phenomics. It is also acknowledged that parameters such as plant height and canopy coverage are dynamic and should not be used indiscriminately. Instead, a more elaborate analysis of seasonal changes is needed. It is also noted that unsupervised classification algorithms used in this study to detect open cotton bolls and canopy from orthomosaic images plays critical roles in the proposed framework, and more thorough investigation on the impact of other classification algorithms may be necessary. Additional research findings regarding UAS-monitored crop growth and development will be addressed in a forthcoming publication.

Acknowledgements

We appreciate Dow AgriSciences for providing materials for field experiments, Rudy Alaniz and Clink Livingston at Texas A&M AgriLife Extension and Kenneth Schaefer at Texas A&M AgriLife Research for their support.

Appendix A. Supplementary material

Supplementary data associated with this article can be found, in the online version, at https://doi.org/10.1016/j.compag.2018.06.051.

References

Rosenfeld, Azriel, Pfaltz, John, 1966. Sequential operations in digital picture processing. J. ACM 13 (4), 471–494.
Araus, J.L., Cairns, J.E., 2014. Field high-throughput phenotyping: the new crop breeding frontier. Trends Plant Sci. 19, 52–61.
Bendig, J., Yu, K., Aasen, H., Bolten, A., Bennertz, S., Broscheit, J., Gnyp, M.L., Bareth, G., 2015. Combining UAV-based plant height from crop surface models, visible, and near infrared vegetation indices for biomass monitoring in barley. Int. J. Appl. Earth Observation Geoinformation 39, 79–87.
Berni, J.A., Zarco-Tejada, P.J., Suárez Barranco, M.D., Fereres Castiel, E., 2009. Thermal and narrow-band multispectral remote sensing for vegetation monitoring from an unmanned aerial vehicle. Inst. Electr. Electron. Eng.
Cabrera-Bosquet, L., Crossa, J., von Zitzewitz, J., Serret, M.D., Araus, J.L., 2012. High-throughput phenotyping and genomic selection: the frontiers of crop breeding converge. J. Integr. Plant Biol. 54, 312–320.
Cobb, J.N., DeClerck, G., Greenberg, A., Clark, R., McCouch, S., 2013. Next-generation phenotyping: requirements and strategies for enhancing our understanding of genotype-phenotype relationships and its relevance to crop improvement. Theor. Appl. Genet. 126, 867–887.
Furbank, R.T., Tester, M., 2011. Phenomics - technologies to relieve the phenotyping bottleneck. Trends Plant Sci. 16, 635–644.
Gago, J., Douthe, C., Coopman, R., Gallego, P., Ribas-Carbo, M., Flexas, J., Escalona, J., Medrano, H., 2015. UAVs challenge to assess water stress for sustainable agriculture. Agric. Water Manage. 153, 9–19.
Gevaert, C.M., Suomalainen, J., Tang, J., Kooistra, L., 2015. Generation of spectral–temporal response surfaces by combining multispectral satellite and

hyperspectral UAV imagery for precision agriculture applications. IEEE J. Sel. Top. Appl. Earth Observations Remote Sensing 8 (6), 3140–3146.
Gómez-Candón, D., De Castro, A.I., López-Granados, F., 2014. Assessing the accuracy of mosaics from unmanned aerial vehicle (UAV) imagery for precision agriculture purposes in wheat. Precis. Agric. 15 (1), 44–56.
Honkavaara, E., Saari, H., Kaivosoja, J., Pölönen, I., Hakala, T., Litkey, P., Mäkynen, J., Pesonen, L., 2013. Processing and assessment of spectrometric, stereoscopic imagery collected using a lightweight UAV spectral camera for precision agriculture. Remote Sensing 5 (10), 5006–5039.
Hulse-Kemp, A.M., Ashrafi, H., Zheng, X.T., Wang, F., Hoegenauer, K.A., Maeda, A.B.V., Yang, S.S., Stoffel, K., Matvienko, M., Clemons, K., Udall, J.A., Van Deynze, A., Jones, D.C., Stelly, D.M., 2014. Development and bin mapping of gene-associated inter-specific SNPs for cotton (Gossypium hirsutum L.) introgression breeding efforts. Bmc Genomics 15.
López-Granados, F., Torres-Sánchez, J., Serrano-Pérez, A., de Castro, A.I., Mesas-Carrascosa, F.J., Peña, J.M., 2016. Early season weed mapping in sunflower using UAV technology: variability of herbicide treatment maps against weed thresholds. Precision Agric. 17 (2), 183–199.
Mayes, S., Parsley, K., Sylvester-Bradley, R., May, S., Foulkes, J., 2005. Integrating genetic information into plant breeding programmes: how will we produce varieties from molecular variation, using bioinformatics? Ann. Appl. Biol. 146, 223–237.
Primicerio, J., Di Gennaro, S.F., Fiorillo, E., Genesio, L., Lugato, E., Matese, A., Vaccari, F.P., 2012. A flexible unmanned aerial vehicle for precision agriculture. Precis. Agric. 13 (4), 517–523.
Rokhmana, C.A., 2015. The potential of UAV-based remote sensing for supporting precision agriculture in Indonesia. Procedia Environ. Sci. 24, 245–253.
Yu, J., Jung, S., Cheng, C.H., Ficklin, S.P., Lee, T., Zheng, P., Jones, D., Percy, R.G., Main, D., 2014. CottonGen: a genomics, genetics and breeding database for cotton research. Nucleic Acids Res. 42, D1229–D1236.